Combustion and its Modeling in Spark-Ignition Engines

J.B.Heywood

Sloan Automotive Laboratory
Massachusetts Institute of Technology
Cambridge, Mass. 02139
USA

ABSTRACT

Our current understanding of spark ignition, flame kernel development, and flame propagation in spark-ignition engines, and our ability to model the critical aspects of these processes, are reviewed. The essential features of these processes are first described to provide a physical basis for the discussion. During flame kernel development, the electrical energy deposited and the heat losses to the spark plug affect the mixture state and, with the mixture composition and flame stretch, govern the initial growth rate. Local bulk convection and turbulence then impact the development of the flame kernel as it transitions to a turbulent flame. The flow turbulence and the flame front/combustion chamber wall interaction then determine the overall behavior of the propagating flame, though mixture composition and state still play a role in the local flame sheet behavior. When the flame reaches the wall, the burnup of mixture locally within the turbulent flame brush continues, governed by the mixture composition and state, and the local turbulence scales.

A framework for examining and evaluating models for these processes is then proposed. The primary factors affecting the charge mass burning rate are the geometry of the flame front/combustion chamber wall interaction, the unburned mixture composition and state, and flow field effects. To model these effects requires first a flame structure model, then a flame speed model. Several models in these two categories have been developed, and the key attributes of the more successful models are described.

The different approaches to modeling the engine flame structure are: mean flame front location models; entrainment and burn up models which describe the behavior of the unburned/burned gas mixture in the turbulent flame brush; and flame sheet models that explicitly describe the engine flame as a thin wrinkled reaction sheet. Two options in this last category are a flame sheet per unit volume approach, and use of the fractals to describe the sheet wrinkling process. How the spark discharge initializes these models is a critical issue. These flame structure models then require laminar and turbulent flame speed models to be able to make engine combustion predictions. These combustion models have been developed for quasi-dimensional phenomenological models of the engine operating cycle and for use in computational fluid dynamic engine computer codes. The paper concludes with some of where these engine combustion models can provide important insights.

INTRODUCTION

This paper reviews our present understanding of the spark-ignition engine combustion process, and describes the different types of engine combustion models currently available. Its focus is on the engine combustion process itself, which starts with ignition by the spark discharge, followed by the development of a small flame kernel which then grows into a turbulent flame and propagates across the engine combustion chamber, finally extinguishing close to the chamber walls. For much of its existence, this flame is a growing unsteady turbulent flame, confined by the specific geometry of the combustion chamber walls and piston crown, with the reactants--the fuel vapor, air, and residual burned gases--essentially premixed.

The combustion process is an especially important part of the engine's operating cycle. Combustion releases the chemical energy of the fuel--the primary source of energy for the engine--in a relatively short time period between the compression and expansion processes, thereby producing the high pressure, high temperature, burned gases which expand within the cylinder transferring work to the piston. A robust combustion process is important for high quality engine operation; the combustion process must be fast, that is occupy a small fraction of the total cycle time so that the engine's energy conversion process is efficient, and highly repeatable so that variations from one cycle to the next are small enough to be barely noticeable.

Combustion is also important for its impact on several other engine characteristics or requirements. The processes by which the engine's emissions form within the cylinder are closely linked with the details of the combustion process. The anti-knock and volatility requirements of the fuel are dictated by the engine combustion process. Even the breathing of the engine, and hence it's power, are affected by what the designer must do to achieve a good combustion process. It is not surprising, therefore, that understanding the engine combustion process, and modeling that process from a fundamental perspective, are such important topics for the engine research community.

The spark-ignition engine combustion process is an extremely complicated combination of phenomena. It involves an arc discharge, the fuel oxidation chemistry, heat losses in a complex geometry, and the role of turbulence over a wide range of length and time scales (1). There is an extensive experimental and modeling literature on engine combustion, and an even more extensive literature on turbulent combustion. At the previous two COMODIA meetings, review papers on engine combustion modeling have been presented (2), (3). Given this wealth of research and review literature, what would a useful additional contribution be? My sense is that in discussions of complex models, the essential features of the real processes that are being modeled are not always adequately described. So while my review, at this third International COMODIA Symposium, is about recent progress in spark-ignition engine combustion modeling, I will focus my paper as much on what we now understand to be the critical

fundamental aspects of the spark-ignition engine combustion process, as on how well currently available models describe these aspects and therefore can be valuable engine development and design tools. I also want to relate these modeling tools to the practical combustion issues that limit engine operation in important ways. First, however, some comments on what we mean by an engine combustion model, and the ways in which models can help engine engineering.

THE VALUE OF ENGINE COMBUSTION MODELING

I will define an engine combustion model as: *a physically based description of the engine combustion process which predicts the mass burning rate and the flame geometry as functions of engine design and operating variables.* We should recognize that due to the complexity of the combustion process, such models are always incomplete to a significant extent, that these models often must incorporate correlations of experimental data, and that the field of combustion modeling is continually developing.

A major and often undervalued role for engineering models is developing useful new knowledge. From that knowledge comes increased understanding of the interactions between the processes and/or the variables involved. There are several critical areas of engine combustion where models can help in this way. For example, while we know largely from experiments how much swirling and tumbling in-cylinder flows improve the combustion process, we do not yet understand the actual processes by which these flows enhance the flame development and propagation processes. Also, our lack of knowledge of the processes by which engine flames slow down and eventually are extinguished, whether during flame kernel development or later in the burning process, still limits our ability to resolve the practical problem of cycle to cycle combustion variations which is what limits lean engine operation and imposes the dilute operating limit for recycled exhaust gas.

The second major combustion modeling opportunity is in engine development and design. These activities need more complete analysis tools which predict the effect of the engine combustion process on engine performance more accurately, by including more of the relevant variables such as the fuel-air mixture preparation system characteristics, the geometric details of the combustion chamber, the major features of the inlet ports, valves, and the in-cylinder flow they produce, and the ignition system parameters. Especially important here is the intended use of the engine combustion model: the level of detail included, the accuracy, and the ease of use must all fit with the intended uses.

These are important research opportunities. They also present us with major challenges. A discussion of what we now understand to be the essential features of the engine combustion process will provide an appropriate background to exploring how ready combustion models are to respond to these needs.

PHYSICS OF THE SPARK-IGNITION ENGINE COMBUSTION PROCESS

The spark discharge generates, on a sub-microsecond time scale, a high temperature kernel of order one millimeter in diameter between the spark plug electrodes. The size of the spark-generated kernel depends on the breakdown energy that the ignition system delivers to the gas. The extremely high discharge generated temperatures of order 60,000 K (4) result in rapid heat conduction to the surrounding gas and the electrodes. The chemical energy of the fuel-air mixture heated by the discharge is released. An outward propagating flame kernel results, as shown in the schlieren photographs of an engine ignition process in Fig. 1, during the first 300 μsec after spark onset (5).

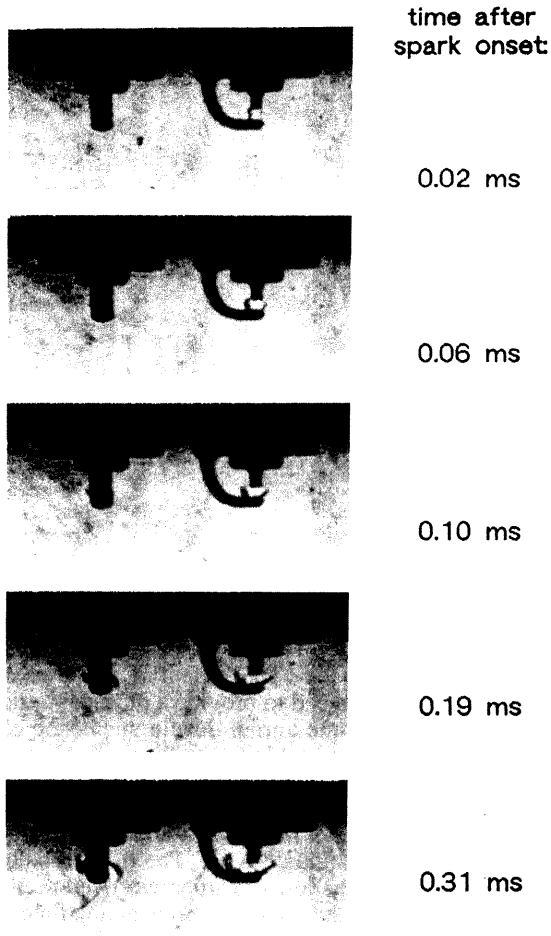

Fig. 1: Schlieren photographs of the spark discharge to flame kernel transition from a single cycle (5). Stoichiometric operation, 1400 rev/min, mixture pressure and temperature at ignition 2 bar and 625 K, respectively. Standard transistorized coil ignition system.

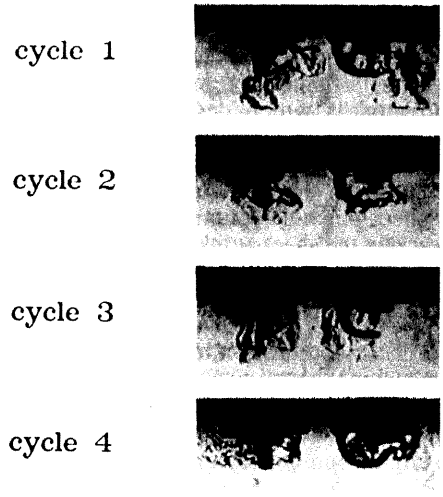

Fig. 2: Schlieren photographs of the growing flame as it transitions to a turbulent flame (5). Four consecutive cycles, 0.84 ms, 7 crank angle degrees, after spark onset. Engine operating conditions as in Fig. 1.

This flame kernel growth is initially laminar like, at least at low to mid-speed engine operating conditions. However, the electrical energy released in the kernel and heat losses from the kernel to the spark plug make this early flame development process non adiabatic (6),(7). Also, when the flame radius is less than or of order 1 mm, flame curvature effects on the growth rate are significant (8).

A gradual transition to a turbulent flame then occurs, as the local flow increasingly distorts the thin laminar-like reaction sheet flame. The local bulk flow can also convect the flame kernel center away from the spark plug electrodes (9)(10). Both these phenomena are apparent in the schlieren photographs in Fig. 2, which shows four consecutive cycles a fixed time (0.84 ms) after spark onset (5). Thus, both the bulk flow and the turbulence in the vicinity of the spark discharge affect this stage of the flame development process. The flame reaction sheet becomes increasingly wrinkled and distorted as the enflamed region grows and the local turbulence at various length scales has time to influence the flame. The convection of the kernel center becomes less significant as the flame grows beyond about 10 mm radius (9) because the enflamed mass is then too large to be transported by the local fluid motion.

The flame propagates outward in an approximately spherical manner from it's center under normal in-cylinder flow conditions. As the flame grows, the flame front contacts the combustion chamber walls and then, locally, quenches. The walls obviously prevent continuing flame growth where the enflamed region is in contact with the combustion chamber walls. Figure 3 shows the flame front location as a function of time during this flame growth and wall interaction period. The engine design and its operating conditions are given in the caption, and are typical. The lines in the figure effectively define the average outer envelope of the now highly wrinkled turbulent flame (10).

Note that to relate these flame contours to the mass fraction of the mixture in the cylinder that has burned, allowance must be made for the difference in density between the unburned gas ahead of the flame and the burned gas behind the flame. For typical engine operating conditions (stoichiometric fuel-air mixture, part-throttle operation), the ratio of the unburned gas density to the burned gas density is about 4 and varies little during the combustion process. Thus, with the spark plug located on the cylinder axis in a disc-shaped combustion chamber, only some 10 percent of the charge has burned when the flame radius is half the cylinder radius.

As the flame kernel grows, the thin reaction-sheet flame is wrinkled by the turbulence motions at scales smaller than the flame radius. Scales of turbulence comparable to and larger than the flame radius only distort the overall flame shape, or convect the flame, respctively. Experimental studies of flame growth (8) show that, once the flame has grown to more than about 5 mm in radius, it can be appropriately described as a turbulent flame. At engine speeds of 1500 to 3000 rev/sec, it takes about 5 to 10 crank angle degrees after spark onset to make this transition. Now turbulent convection is the dominant transport process, and the flame speed approaches that of a freely propagating developed turbulent flame (11).

Figures 4 and 5 show results from three types of experimental approaches often used to visualize engine flames in their turbulent stage. Figure 4 is a schlieren image of a turbulent engine flame in a square-cross-section visualization engine in the author's laboratory which has been used in many studies of flame propagation (1). The flame shown started at

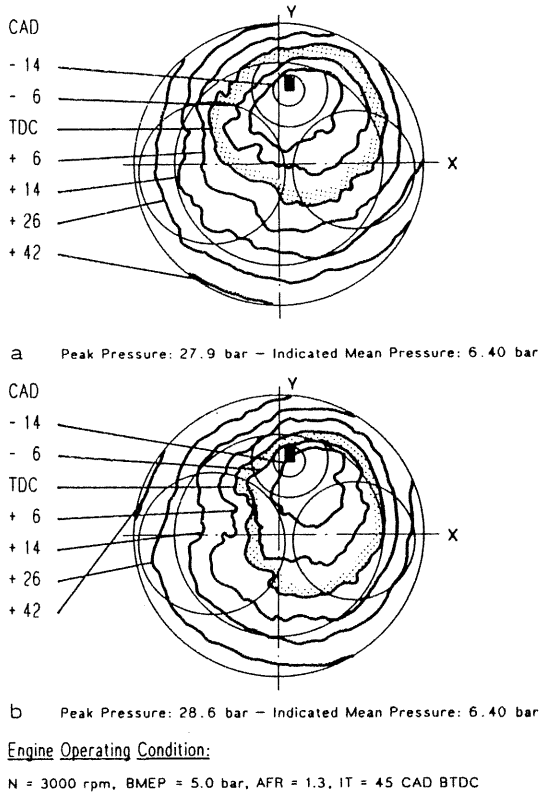

Fig. 3: Flame contours illustrating flame propagation in two cycles with nearly identical cylinder pressure histories (10). Flames detected with high-speed schlieren cinematography, and with multi-ionization probes in that part of the cylinder head which is not optically accessible. Note the approximately spherical outer shape of the flame.

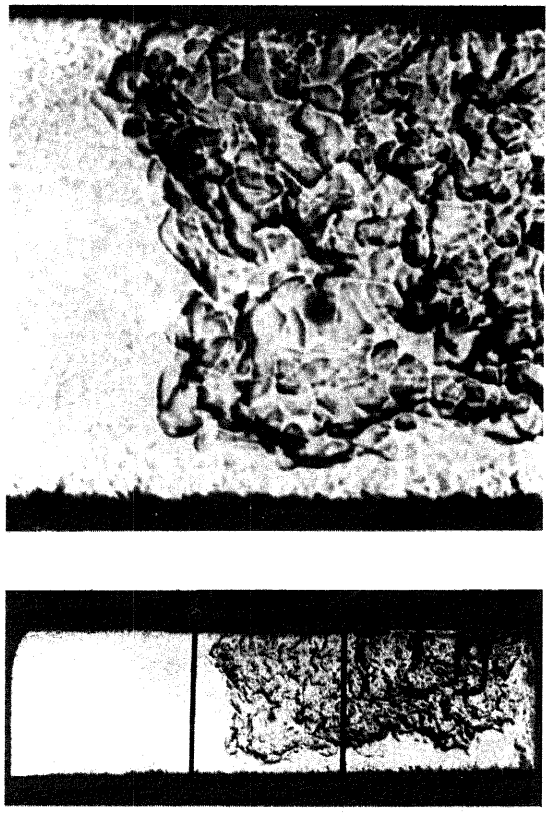

Fig. 4: Schlieren photograph of the turbulent, wrinkled reaction-sheet, spark-ignition engine flame (1). Lower photo shows the full square-cross-section engine combustion chamber; upper photo shows the center portion enlarged. Operating conditions: stoichiometric, propane fuel, 1400 rev/min, 0.5 bar inlet pressure.

the spark plug electrode gap on the right-hand side of the lower photo, and is propagating downwards towards the piston crown and to the left towards the far cylinder wall. A portion of this photo is shown enlarged at the top. Schlieren photographs are integrated images along the optical path of the parallel light beam. Given that this flame is propagating outward in a roughly spherical manner, the schlieren image of the flame moving to the left can be interpreted as a tangential view of the turbulent wrinkled reaction-sheet flame where those sheet regions that have moved ahead of the mean sheet location appear as "hills," stacked beside and behind each other on the "horizon." That portion of the schlieren image which is viewed perpendicular to the plane of the mean flame front appears as an "aerial view" of "hilly terrain" where the "bottoms of the valleys" appear as lines. A feature of the wrinkled flame-sheet model, where the turbulence distorts and convolutes the reaction sheet, is that the local laminar forward diffusion of the sheet rounds the leading flame sheet regions and forms cusps at the trailing flame sheet regions.

Figure 5 shows simultaneous images obtained from flame radiation, and planar laser-induced fluorescence of unburned hydrocarbon, in an optically accessible spark-ignition engine with a disc-shaped combustion chamber (12). The flame radiation technique produces an outer flame image similar to that produced by the schlieren technique. Two-dimensional planar imaging of flames has become a well-developed and valuable technique for examining the details of the flame structure (e.g., see (13)). The example shown, which identifies the unburned mixture region in a plane through the clearance height, shows finger-like regions of unburned gas that have penetrated into the turbulent flame and similar regions of burned mixture that have moved ahead of the mean reaction-sheet location. These two-dimensional planar images usually show a more irregular boundary between the burned and unburned regions than is apparent with the schlieren visualization technique used in Figs. 2 and 4.

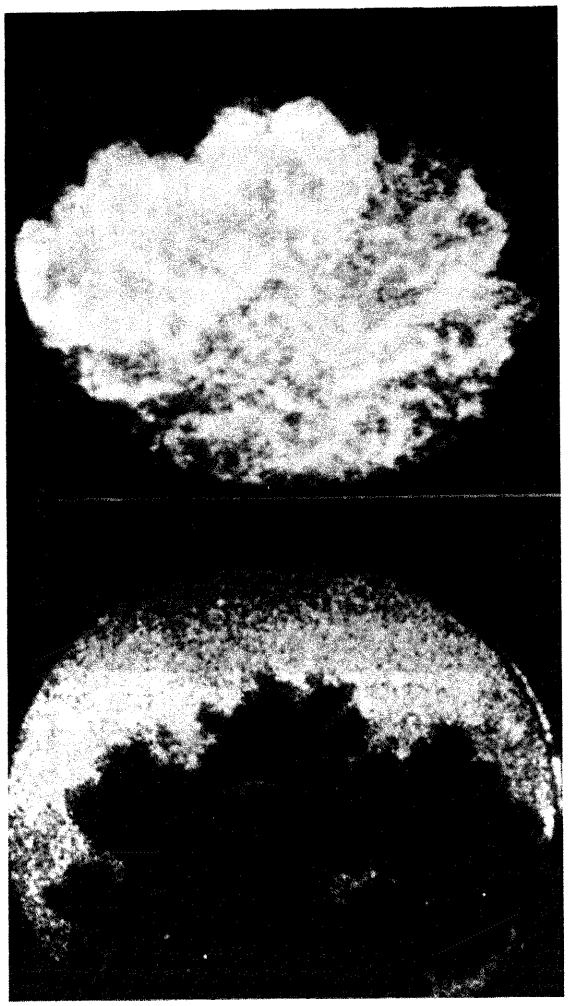

Fig 5: Simultaneous imaging of flame radiation (top) and planar laser-induced-fluorescence of unburned hydrocarbon fuel (12). Image timing is 4 deg. before top center; imaging plane is through the disc-shaped clearance volume.

The turbulent spark-ignition engine flame is normally in the wrinkled reaction sheet regime of turbulent combustion (14). The turbulent Reynolds number is in the 100-1000 range. The Damkohler number, which is the ratio of the eddy turnover time to the residence time in the laminar flame, is of order 100 (fast chemistry regime), and the smallest turbulent eddy size is larger than the laminar flame thickness so the reaction sheet structure is little affected by the turbulence. The turbulence wrinkles and distorts the flame, increasing the amount of thin reaction sheet contained within the turbulent flame zone (often called the flame brush) by a factor which is substantial and which increases with increasing turbulence. Most importantly, this wrinkling increases the mass burning rate. An opposing effect which wrinkling also produces is the stretching of the flame sheet which slows down the molecular diffusive processes within the flame. Whether this effect is significant depends on strain rate and mixture composition.

It is now well established (15),(16) that the turbulence intensity u'--the root mean square value of the fluctuating velocity-- at time of combustion, has a value equal to about half the mean piston speed. Hence, the ratio of reaction sheet area (often called the laminar flame area) to the turbulent flame frontal area (for which flame envelope area is a useful term) increases with increasing engine speed. It is primarily for this reason that the mass burning rate which is proportional to the reaction sheet area, increases almost linearly with engine speed, thereby maintaining the angle required to burn from 10 to 90 percent of the in-cylinder charge almost constant over the full speed range of the engine. This laminar to turbulent flame area ratio typically has a value of about 10 at 2000 rev/min.

The final stage of combustion, when the flame approaches the wall and extinguishes, has been much less extensively examined. There is a literature on laminar flame quenching at a cool wall leading to the formation of quench layers--a thin layer of unburned fuel air mixture adjacent to the wall (see (1)). It is often assumed that the local (laminar) regions of the wrinkled turbulent flame that come in contact with the wall quench as described above while the remainder of the turbulent flame brush burns out as if the wall is not there. This inherently assumes that the unburned gas thermal boundary layer thickness is small relative to the turbulent flame thickness. However, as the flame approaches the wall, only successively smaller scales of turbulence are available to affect the flame so the final burn up process may be slower than would occur in the developed turbulent flame (17).

CHARACTERIZATION OF ENGINE COMBUSTION MODELS

In terms of the engine *combustion system*--the chamber geometry and plug location, and the intake port and valve geometry which determines the in-cylinder flow during combustion--the primary quantities of interest are:

(1) The mass burning rate of the unburned mixture since this, through energy conservation, is directly linked to the cylinder pressure and hence engine performance.
(2) The cycle-by-cycle variation in the mass burning rate since this, via torque fluctuation, determines the stability of engine operation.
(3) The burned gas heat transfer areas which have a significant, though secondary, effect on the above energy balance.

At a more fundamental level, the factors that affect the mass burning rate are (18):

(1) The mean flame frontal (or envelope) area contained within the boundaries of the combustion chamber.
(2) The relevant bulk and turbulence flow parameters during combustion--the local mean flow, the local turbulence intensity, and the wrinkling length scales.
(3) The local unburned mixture composition and state, which determine the local laminar burning velocity.

It is the combining together of physically-based relations that define these factors, to predict the mass burning rate and flame geometry, that is the purpose of the engine combustion model. The turbulent engine flame the combustion model must describe is the wrinkled laminar flame described in the previous section. The parameters which define the structure and propagation speed of this flame are summarized in Fig. 6, where a two-dimensional schematic of the flame is shown (16). The turbulent flame contour is drawn as a thin reaction sheet, wrinkled or convoluted at various length scales. The mean flame contour is indicated, as are the mean "front" and "back" of the flame. The turbulent flame speed, S_T, is the velocity at which the mean flame contour propagates into the unburned mixture ahead of the flame. Locally, each point of the thin reaction sheet propagates forward into the unburned mixture ahead of it at the local laminar flame speed, S_L. S_L depends on the unburned mixture composition (fuel composition, relative air/fuel ratio, and residual or burned gas fraction), mixture temperature and pressure, and under certain operating conditions on the flame stretch due to both curvature and turbulence.

The various turbulence length scales can be related to this description of the spark-ignition engine flame. For the wrinkled flame description to be valid, the Kolmogorov scale of the turbulence, the eddy size at which molecular viscosity becomes important, must be larger than the laminar flame thickness so that the laminar flame structure is essentially unperturbed. Estimates based on turbulence measurements indicate that this is usually the case (8),(13),(15)-(17). Until the flame radius is of the order of the integral scale, the size of the major energy containing eddies in the turbulent flow, the impact of turbulence on the flame reaction sheet is limited (19). Once the flame is significantly larger than this size, the largest and smallest scales between which the turbulence wrinkles the flame are this integral scale, and Kolmogorov scale or the Gibson scale (a scale deduced from dimensional arguments to be the minimum vortex size that can significantly wrinkle the flame sheet). These two scales in engines are typically a few millimeters, and about 0.1 mm or less, respectively. These length scales decrease with increasing engine speed. The maximum wrinkling occurs mid way between these scales (8).

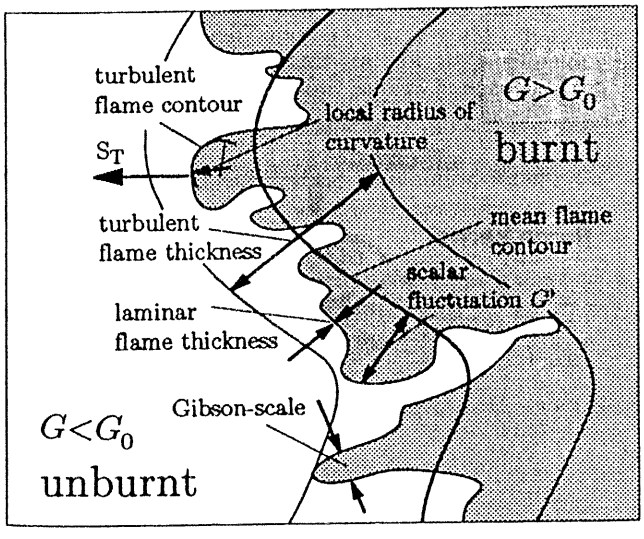

Fig. 6: Schematic of wrinkled turbulent flame structure, showing the characteristic parameters and length scales (16).

As already noted, an additional important impact of the turbulence is the local stretching or straining of the reaction sheet that this flame wrinkling produces. Flame straining is usually quantified by the product of the Lewis number, Le, and the Karlovitz stretch factor, K. The Lewis number is the ratio of thermal diffusivity α to molecular diffusivity D; i.e. Le = α/D. The Karlovitz stretch factor is the product of the turbulent strain rate and the transit time, τ_L, for flow through the laminar flame: i.e.

$$K = (\frac{1}{A_L}\frac{dA_L}{dt})\tau_L = (\frac{u'}{l_T})(\frac{\delta_L}{S_L}) \qquad (1)$$

where A_L is the laminar flame area, u' is the turbulence intensity, l_T is the Taylor microscale of the turbulence, δ_L is the laminar flame thickness, and S_L is the laminar flame speed. The higher the value of the product (LeK), the more important is the impact of flame stretch on the laminar burning velocity. At high enough values of this product, the flame can be quenched (20)(21). Under normal engine operating conditions, this effect is small (Le is about 1 for stoichiometric mixtures, and K is of order 0.1). Lean mixtures increase Le above unity, and high engine speeds increase the amount of stretch; at the lean operating limit these combined effects are the likely cause of misfire, i.e., the extinguishing of the flame.

Table 1 gives values for the parameters, velocities and the length scales, that characterize this engine flame under typical operating conditions. Note that u' and S_T increase with increasing engine speed--which of course is the reason why the duration of the main part of the engine's combustion process expressed in crank angle degrees only modestly increases with engine speed. The turbulence length scales decrease with increasing speed, as one expects from basic turbulence relationships.

Previously, the author (23), based on a discussion of the inherent dimensionality of engine combustion models by Bracco (24), has suggested that computer models used to

Table 1: Typical Values of Quantities which Characterize Engine Flames

Speed = 1500 rev/min; stoichiometric mixture

Turbulence intensity, u'	2 m/s
Turbulent Reynolds No., Re_T	300
Damkohler No., Da	20
Karlovitz Stretch Factor, K	0.2
Integral scale, l_I	2 mm
Taylor Microscale, l_T	0.7 mm
Kolmogorov Scale, l_K	0.03 mm
Gibson Scale, l_G	0.2 mm
Laminar Flame Thickness, δ_L	0.02 mm
Laminar Flame Speed, S_L	0.5 m/s
Ratio u'/S_L	4
Ratio S_T/S_L	4
Mean Flame Radius of Curvature	2 mm

Values taken from references (16), (17), (22)

predict engine performance be classified as zero-dimensional, quasi-dimensional, or multi-dimensional, depending on how critical processes such as combustion are related to the in-cylinder flow field. Zero-dimensional models are based on the equations of thermodynamics, do not involve any flow-field details, and are primarily of value in analyzing the energy conversion aspects of internal combustion engines. Multi-dimensional models are based on the solution of the Navier-Stokes equation, and directly relate in-cylinder processes to the details of the in-cylinder flow. To date these models have been used more to develop our understanding of critical engine processes than to predict the engine's operating characteristics. A primary reason for this research emphasis in the use of multi-dimensional models is their extensive computer time requirement. Quasi-dimensional models were developed to bridge the gap between the zero and multi-dimensional models. They introduce a spatial dependence into processes such as combustion and heat transfer in an explicit phenomenological manner, rather than deriving that spatial dependence from the solution of the full set of conservation equations. Quasi-dimensional models are useful because they do relate the model outputs to the combustion chamber geometry and aggregate flow field parameters, and the computer running times are modest.

What combustion models do these engine simulations require? Simple empirically-based combustion models are all that is needed in zero-dimensional simulations. Quasi- and multi-dimensional simulations require models for flame initiation, development and propagation. All engine combustion models have two distinct parts: a flame structure model and a flame speed model. The flame structure models are approximations to the schematic of the turbulent wrinkled reaction-sheet flame illustrated in Fig. 6. The flame structure model then requires values for the flame speed: laminar, turbulent, and the transition between these. The flame speed model provides these values. The next two sections describe the more commonly used types of engine flame structure and flame speed models.

FLAME STRUCTURE MODELS

Mean Flame Front Models

The simplest flame structure model is to represent the turbulent flame shown schematically in Fig. 6 by its mean location. More precisely, this mean contour is the surface obtained by averaging out the turbulent fluctuations in the scalar variable G, where G_0 represents the actual flame surface and $G < G_0$ defines unburned mixture and $G > G_0$ defines burned mixture (16). The mass burning rate is given by

$$\frac{dm_b}{dt} = A_f \rho_u S_f \qquad (2)$$

where m_b is the mass of charge burned, A_f is the mean flame area, ρ_u is the unburned mixture density, and S_f is the flame speed (laminar or turbulent).

In quasi-dimensional engine cycle simulations, this approach to flame structure also requires a flame geometry model. Often an expanding spherical mean-flame surface is assumed, centered at the center of the enflamed region and cut off as appropriate by the combustion chamber walls. The flame center is often assumed to be the spark plug electrode gap location. This ignores the fact that flame kernel convection by the local bulk flow can be significant while the flame is small. When this type of model is used to follow the development of the flame kernel, spherical expansion is usually assumed initially, with either a transition to an ellipsoidal outer kernel boundary (25) or a continuous generation of new flame kernels (11) to account for the convection of the kernel center and the flame holding effect of the spark plug electrodes.

Quasi-dimensional combustion models of this type then use mass and energy balances for an open thermodynamic system whose boundary coincides with the expanding mean flame contour. The energy transfers for this system are shown in Fig. 7 for the early stages of flame development, when the energy and mass conservation equations are (25):

$$dU = h_u dm_b + dE_{sp} - \delta Q_{ht} - pdV_b \qquad (3)$$

where U is the internal energy of the gas in the kernel, h_u is the enthalpy of the gas entering the open system, dm_b is the incremental burned mass that enters the kernel due to combustion, dE_{sp} is the energy gain due to the spark discharge (important when the flame is small), δQ_{ht} is the heat transfer to the walls, and pdV_b is the work transfer due to flame expansion. This, with the mass balance equation (2) leads to an equation for the rate of change of mean burned gas temperature, T_b,

$$\frac{dT_b}{dt} = \frac{(h_u - h)}{c_p \rho_b} \frac{A_f}{V_b} S_f + \frac{(\dot{E}_{sp} - \dot{Q}_{ht})}{c_p \rho_b V_b} + \frac{1}{c_p \rho_b} \frac{dp}{dt} \qquad (4)$$

and an expression for the burned gas volume

$$\frac{dV_b}{dt} = \frac{\rho_u}{\rho_b} A_f S_f + V_b \left(\frac{1}{T_b} \frac{dT_b}{dt} - \frac{1}{p} \frac{dp}{dt} \right) \qquad (5)$$

Initially, the flame speed S_f in Eqs. (4) and (5) is the laminar flame speed, appropriately incorporating the effects of electrical energy deposition and heat loss on the flame kernel temperature, and flame-curvature produced strain. As the kernel grows, it transitions to a turbulent flame. Models for the flame speed in these different regimes of flame development are reviewed in the next section.

Kernel Initiation

The initialization of this flame kernel development process is an especially difficult modeling problem. The breakdown phase of the spark discharge (in 10 - 100 nanosec) creates a narrow channel of highly ionized plasma with initial temperatures of order 60,000 K (4). The spark-generated plasma then cools on a microsecond timescale through heat conduction to the surrounding gases. The mixture chemical energy that has been released within the kernel then becomes significant. Maly et al (11) and Sher et al (26)(27) have developed models for this total process which essentially incorporate each individual process, one at a time in sequence

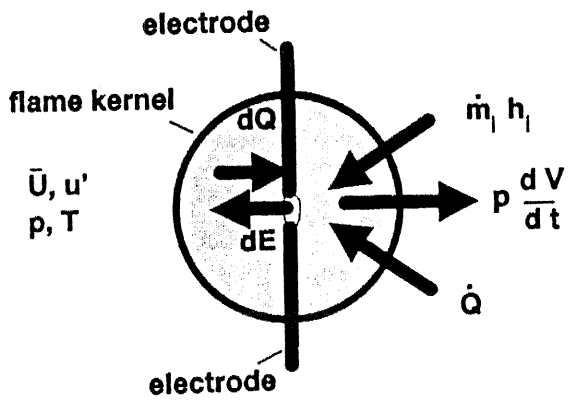

Fig. 7: Open thermodynamic system boundary for the mean flame contour model of the developing flame (11).

on the appropriate time scale, to predict an initial spark-generated flame kernel size and kernel gas temperature, based largely on the electrical energy deposited during the breakdown ignition phase. It turns out that these initializing parameters are not especially sensitive to the simplifying assumptions made because the spark kernel size for a given breakdown energy, once established, varies only modestly with time in the 1 - 100 microsec time period.

Entrainment and Burn-Up Flame Models

In this type of flame structure model, the mixture burning process is described as occurring in two stages. First, unburned mixture is entrained into the turbulent flame brush; then, burn up within the flame brush occurs at a rate governed by the amount of unburned mass within the flame divided by a characteristic burning time. This burning time τ_b, based on the flame structure illustrated in Fig. 6, is equated to the characteristic size of the entrained eddies divided by S_L, the local laminar flame speed. Since this concept was first applied to engine flames by Blizard and Keck (28), these so-called entrainment models have been extensively used in quasi-dimensional simulations of engine operation. These models have also been expanded to include more of the relevant physics: see (19),(29)-(34).

The combustion process is described by the following differential equations which apply to the mean outer flame contour in Fig. 6:

$$\dot{m}_e = \rho_u A_f S_f \tag{6}$$

$$\dot{m}_b = \frac{m_e - m_b}{\tau_b} + \rho_u A_f S_L \tag{7}$$

where

$$\tau_b = c\ell_e / S_L \tag{8}$$

m_e is the total mass entrained by the outer flame envelope surface; m_b is the total burned mass; ρ_u, ρ_b are the densities of the unburned and burned gases, respectively; A_f is the area of the (spherical) flame front required to entrain m_e; ℓ_e is the length scale of the entrained eddies; S_f is the total flame speed; S_L is the laminar flame speed; τ_b is the characteristic time for eddy burn-up; c is an empirical constant ($\approx$ 2.5 (34)). The length scale in Eq. (8) is frequently taken to be the Taylor microscale.

Note that this type of model does need to be calibrated against experimental data. The calibration constants are of order unity, however. With quasi-dimensional engine simulations, as with the mean flame front models, entrainment and burnup models require a geometric model for the flame front. Often, a simple spherical assumption for the flame envelope surface is made.

Flame Sheet Models

An alternative modeling approach to the flame structure illustrated in Fig. 6 is to estimate the surface area of the wrinkled thin reaction-sheet flame, A_L. The mass burning rate is then given by

$$\frac{dm_b}{dt} = \rho_u A_L S_L \tag{9}$$

Thus, from Eq. (2), the ratio S_f / S_L is given by:

$$S_f / S_L = A_L / A_f \tag{10}$$

We will illustrate two approaches employed to estimate the laminar flame or reaction sheet area: the use of the fractal geometric model to describe the wrinkled flame surface, and the coherent flame sheet model which calculates the flame sheet area per unit volume.

The fractal model assumes self similarity between scales of different size, which results in a power-law scaling between measured size and measurement scale. This is illustrated in Fig. 8, where the measured surface area, A, is plotted versus the measurement scale, ε, using log-log scales. One obtains a straight line of slope 2 - D. When applied to turbulent flames, there are physically imposed smallest and largest scales. Both the Kolmogorov and the Gibson scales have been proposed as the smallest scale or inner cut off, as discussed in the previous section. The outer cut off is usually taken to be the integral scale of the turbulence (35),(36). Then, from Fig. 8,

$$\frac{S_f}{S_L} = \frac{A_L}{A_f} = \left(\frac{\ell_K}{\ell_I}\right)^{2-D} or, = \left(\frac{\ell_G}{\ell_I}\right)^{2-D} \tag{11}$$

To use this model, an equation for the fractal dimension, D, and expressions for the inner and outer cut offs are required. The laminar flame speed, including the effect of flame stretch if that is important, must also be described. Santavicca et al (36) propose the relation

$$D = \frac{2.0 S_L}{u' + S_L} + \frac{2.35 u'}{u' + S_L} \tag{12}$$

for the fractal dimension, based on data that showed that D increases from 2 for a laminar flame to about 2.35 for highly turbulent flames, as shown in Fig. 9 (36).

Various assumptions about the smallest and largest length scales for use of this fractal model in engines have been tested (37),(38). The best agreement with experimental data was obtained with the ratio ℓ_{max} / ℓ_{min} given by ℓ_I / ℓ_K. Standard turbulence relationships are used to estimate these length scales. Encouraging results in terms of cylinder pressure predictions over a range of engine speeds have been obtained (38). The initialization of the flame still needs additional physically-based input. It was found that the decay of turbulence in the boundary layer must be included to simulated the decrease in burning rate as the flame approaches the wall.

A flame sheet approach used in multi-dimensional or computational fluid dynamic engine codes, the coherent flame sheet model, is based on calculating the reaction sheet surface

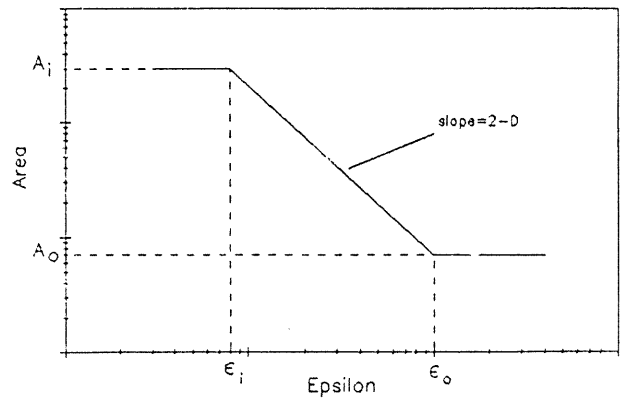

Fig. 8: Theoretical fractal behavior of the area of a wrinkled surface as a function of measurement scale, on a log-log plot. A straight line of slope 2 - D is obtained between the inner and outer cutoff scales (15).

area per unit volume in the turbulent flame. The fundamental assumption is made that the reaction sheet thickness is small compared to the energy-containing turbulent eddies in the turbulent flame illustrated in Fig. 6. The flame sheet model then describes how the flame surface density--sheet area per unit volume, Σ, evolves with time, in the turbulent flame brush. This flame surface density is initiated by spark ignition, sustained by turbulent straining, convected by the bulk gas motion, and either consumed by laminar flame propagation or extinguished by over straining. The following description of this coherent flame sheet model is by Cheng and Diringer (39).

Since the flame is an "active" surface, its evolution is modeled by assuming that the flame surface generation rate is proportional to the local average magnitude of the strain rate e (with a proportionality constant α of order 1 to 10):

$$\frac{D\Sigma}{Dt} = \alpha e \Sigma \tag{13}$$

The mean strain rate e may be calculated from the turbulence model.

When the strain rate exceeds a critical value e_s, the flame surface may be locally extinguished by over-straining. The rate of destruction of the flame surface would be proportional to the amount of over-straining, i.e.,

$$\frac{D\Sigma}{Dt} = \begin{Bmatrix} -\gamma(e-e_s)\Sigma & for\ e > e_s \\ 0 & for\ e < e_s \end{Bmatrix} \tag{14}$$

where γ is the proportionality constant.

The combustion process proceeds with the laminar consumption of the mixture by the flame sheet. If Y_1 is the local unburned mixture mass fraction and ρ the charge density, the burning rate is given by

$$\frac{D\rho Y_1}{Dt} = -\rho_u S_L \Sigma \tag{15}$$

The destruction of the flame sheet density by burning is

$$\frac{D\Sigma}{Dt} = -\frac{\beta\Sigma}{\tau_b} = -\frac{\beta\rho_u S_L \Sigma^2}{\rho Y_1} \tag{16}$$

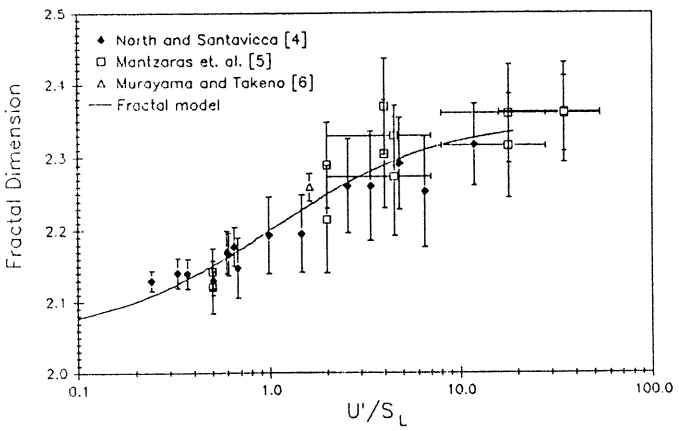

Fig. 9: Comparison of the fractal dimension D for turbulent flames, predicted by Eq. (12), with experimentally measured values (15). Note the transition from D = 2 for a laminar flame to 2.35 for a fully turbulent flame.

where τ_b is a characteristic burning time given by ℓ / S_L, and ℓ is the "thickness" of the unburned layers: $\ell = (\rho Y_1 \rho_u \Sigma)$. β is a proportionality constant. The burn-out is fast when there is not much mixture left (small ρY_1).

The flame sheet is transported by convection, which may be decomposed into two components, bulk convection and turbulent diffusion. The latter may be modeled with a turbulent diffusivity D_Σ

$$D_\Sigma = c_\Sigma k^2 / (\rho\varepsilon) \tag{17}$$

where k is the turbulent kinetic energy and ε its dissipation rate.

The evolution of the flame density Σ is then given by the following equations.

$$\frac{\partial\Sigma}{\partial t} + \nabla\bullet(u\Sigma) = \frac{1}{\rho}\nabla\bullet(\rho D_\Sigma \nabla\Sigma) + s\Sigma - \frac{\beta\rho_u S_L \Sigma^2}{\rho Y_1} \tag{18}$$

where

$$s = \begin{Bmatrix} +\alpha e & for\ e < e_s \\ -\gamma(e-e_s) & for\ e > e_s \end{Bmatrix} \tag{19}$$

Flame Structure Model Summary

This section has summarized the basic types of flame structure models used for spark-ignition engine combustion analysis. There are, of course, variants from the models discussed above. For example, turbulent combustion models which use probability density functions (PDFs) to descibe the distribution of the burned and the unburned gas within the flame, have been developed for multi-dimensional codes (40)-(42). The physical basis for this approach is that the turbulent flame brush consists of regions or pockets of fully burned gas, or pockets of fully unburned gas, separated by a thin reaction sheet. Thus the PDF approach has similarities to the flame sheet area per unit volume model, already described. Somewhat surprisingly, most of the different flame structure models reviewed above have been used in both quasi-dimensional and multi-dimensional/computational fluid dynamic engine simulations.

FLAME SPEED MODELS

Laminar Flame Speed Models

The initial flame kernel growth is laminar. The most commonly used relationships for the adiabatic laminar flame speed are those derived from spherical combustion bomb measurements by Metgalchi, Keck, and Rhodes (43)-(45). They have the form:

$$S_L = S_{L,o}\left(\frac{T_u}{T_o}\right)^\alpha \left(\frac{p}{p_o}\right)^\beta \tag{20}$$

where $S_{L,o}$, α and β, are constants for a given fuel and fuel/air equivalence ratio. These correlations are based on data obtained with practical fuels--propane, indolene, and methanol; the data were taken at unburned mixture temperatures and pressures relevant to spark-ignition engines. The effect of fuel/air equivalence ratio on S_L is shown in Fig. 10.

An important factor in the laminar flame speed correlation is the burned gas fraction in the unburned mixture--the residual gas plus any recycled exhaust (45): see Fig. 11. The data in Fig. 11 are correlated by

$$S_L(\tilde{x}_b) = S_L(\tilde{x}_b = 0)(1 - 2.06\tilde{x}_b^{0.77}) \qquad (21)$$

where $\tilde{x}_b$ is the mole fraction of burned gas diluent. A review of other approaches to modeling laminar flame speeds can be found in ref. (46).

The developing flame kernel is not adiabatic, however; also when it is small ($\leq$ 2 mm) flame curvature effects can be significant. For non-adiabatic flames, the burned gas temperature is no longer just a function of the unburned mixture composition and state. The laminar flame speed depends on the temperature gradient across the flame. Thus, non-adiabatic laminar flame speed models must either incorporate the actual burned gas temperature directly, or the energy transfers (spark energy and heat loss) that make the flame non-adiabatic. Pischinger and Heywood (25) found that, for a given unburned mixture state prior to combustion, the laminar flame speed scaled linearly with burned gas temperature as

$$S_L = S_{L,ad}(T_f - T_q)/(T_{ad} - T_q) \qquad (22)$$

where T_f is the flame kernel temperature, T_{ad} is the adiabatic flame temperature, and T_q is a "quenching temperature" (i.e., the temperature at which the burning velocity becomes zero). T_q was found to be about 1600 K for normal engine compression temperatures. An alternative formulation by Boulouchos et al (8) relates the difference between the non-adiabatic and adiabatic laminar flame speeds to the net energy deposition (electrical energy into the kernel minus heat losses out) divided by the heat of reaction.

Flame curvature for a small spherical flame may slow down the burning rate. Markstein (47) has suggested a linear dependence of laminar flame speed on flame stretch:

$$S_{L,s} = S_{L,ad} - Ma\delta_L k_s \qquad (23)$$

where $S_{L,s}$ is the stretched laminar flame speed, δ_L is the flame thickness, Ma is the Markstein number (which describes the sensitivity of the flame's laminar burning velocity to stretch), and k_s is the flame stretch defined by:

$$k_s = \frac{1}{A_f}\frac{dA_f}{dt} \qquad (24)$$

k_s is equal to $(2/r_f)(dr_f/dt)$ for a spherical growing flame; r_f is the flame radius (8). Markstein numbers range typically from about 2 to 6 (16). Flame curvature effects on early flame development can be substantial (8).

Turbulent Flame Speed Models

There are a large number of turbulent flame speed models. Here, we focus on models that have been used in spark-ignition engine combustion simulations. Models for the turbulent burning velocity of the form:

$$\frac{S_T}{S_L} = 1 + c\left(\frac{u'}{S_L}\right) \qquad (25)$$

where c is a constant or involves a limited number of scaling parameters, have proved surprisingly useful. Entrainment and burn up models often use this type of relationship for the flame front velocity; for example ref. (34) used:

$$\frac{S_f}{S_L} = 1 + C\left(\frac{\rho_u}{\rho_b}\right)^{1/2}\left(\frac{u'}{S_L}\right)(1 - e^{-r_f/r_c}) \qquad (26)$$

where r_f is the flame radius, r_C is of the order of the turbulence integral scale ℓ_I, and C is a coefficient of order 1. Equations like Eq. (26) are intended to predict flame speeds

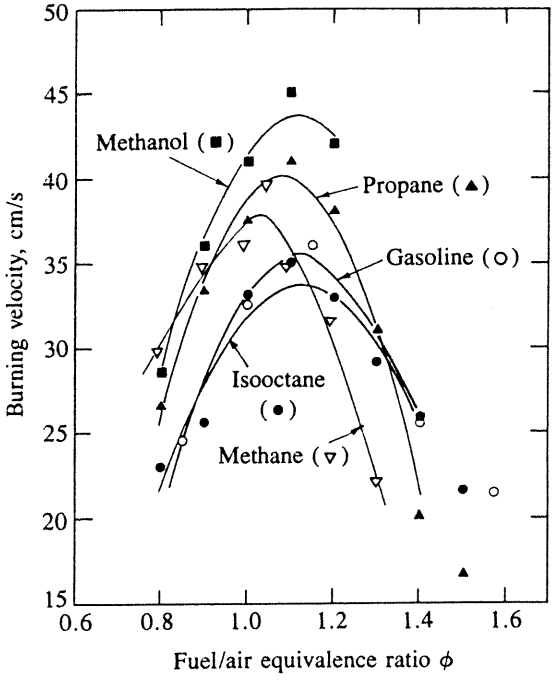

Fig. 10: Laminar burning velocity for several different fuels as a function of fuel-air equivalence ratio, at 1 atm and 300 K (1).

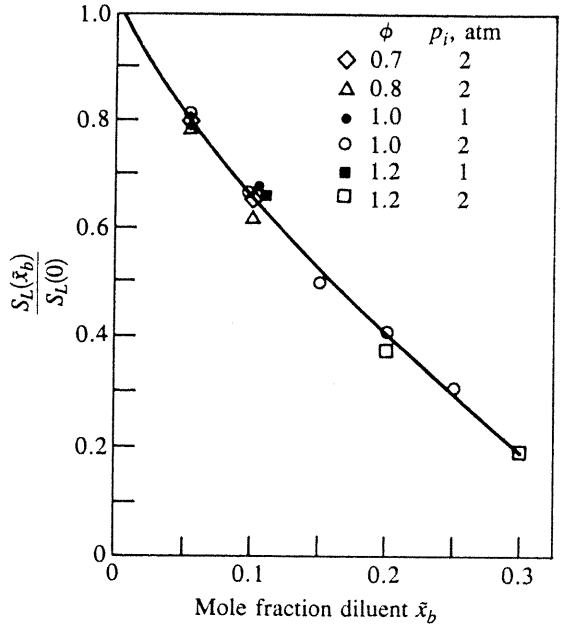

Fig. 11: Effect of burned gas mole fraction x_b in the unburned mixture on laminar burning velocity. Fuel is gasoline (1).

for the initially laminar-like flame kernel ($r_f << r_c$), through to a fully developed turbulent flame ($r_f >> r_c$).

Flame speed models are often correlations of experimental flame-speed data with physically-based dimensionless scaling relationships. The work of Bradley, Sheppard and co-workers at Leeds University is a good example of this approach (17),(20),(21). The turbulent burning velocity, the velocity at which the mean flame contour in Fig. 6 propagates into the unburned gas, expressed as a flame speed ratio S_T / S_L, is correlated with the normalized turbulence intensity u' / S_L, and the product of the Karlovitz stretch factor K and the Lewis number Le. Figure 12 shows how smoothed data from a large number of experiments can be correlated in this manner (17). High values of the product KLe, to the right of the diagram, can result in flame quench.

To include the transition from a laminar to turbulent flame, this group has developed the concept of "effective" turbulence intensity u'_K. The normalized power spectral density of the turbulence is integrated with respect to frequency up to the reciprocal of the time elapsed since ignition to obtain this effective turbulence intensity. The ratio u'_K / u' so obtained then defines how turbulent the developing flame is on the flame speed plot, Fig. 12 (17). This is analagous to the concept that only turbulence scales significantly smaller than the flame size can wrinkle the flame.

A flame speed model which attempts to incorporate the underlying physics in the engine's developing turbulent flame in a more complete manner has been developed by Herweg and Maly (11). The model encompasses the following stages of flame evolution: spark ignition and flame kernel initiation; passage through a flame speed minimum (the initial accelerating effect of the electrical discharge energy decreases before the accelerating effect of the turbulence is fully felt); increasing wrinkling of the flame front as the flame becomes turbulent; and, finally, fully developed turbulent flame propagation. This is, as proposed, a combined flame structure and flame speed model the flame structure model is the mean flame contour model of Fig. 7. Through an extensive analysis of the important physical processes involved, the following expression for the flame speed ratio S_f / S_L is obtained:

$$\frac{S_f}{S_L} = \underbrace{I_0 + I_0^{1/2}}_{\text{I: strain}} \quad \underbrace{\left(\frac{\left[\overline{U}^2 + u'^2\right]^{1/2}}{\left[\overline{U}^2 + u'^2\right]^{1/2} + S_L} \right)^{1/2}}_{\text{II: effective turbulence factor}}$$

$$\underbrace{\left(1 - \exp\left(-\frac{r_f}{\ell_I}\right)\right)^{1/2}}_{\text{III: size dependent integral length scale}}$$

$$\underbrace{\left[1 - \exp\left(-\frac{t}{\tau_0}\right)\right]^{1/2}}_{\text{IV: time dependent integral time scale}} \quad \underbrace{\left(\frac{u'}{S_L}\right)^{5/6}}_{\text{V: fully developed turbulent combustion}} \qquad (27)$$

Here, I_o represents the effect of strain on the laminar burning velocity, $\overline{U}$ is the mean flow velocity, r_f is the flame radius, ℓ_I is the integral scale of the turbulence, t is time after spark onset, and τ_o is a characteristic timescale over which the larger scales of the flow affect burning given by $\ell_I / [(\overline{U}^2 + u'^2)^{1/2} + S_L]$. The relevant physical processes are incorporated as follows: non-adiabatic effects enter through S_L; flame straining effects are represented by terms I (flame curvature) and II (turbulent wrinkling of the reaction sheet); flame growth through the laminar to turbulent flame transition by terms III and IV; the fully developed effect of turbulence by term V.

This model has been applied to the developing flame kernel in special transparent engine facilities with considerable success: an example of the results will be shown in the next section.

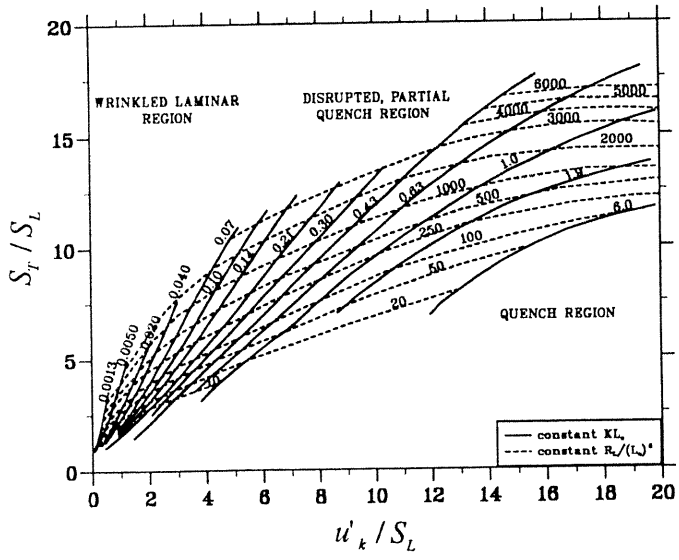

Fig. 12: Turbulent burning velocity diagram (17). Smoothed measurements of S_T / S_L are plotted against u'_k / S_L at different stretch rates. Solid lines are lines of constant Karlovitz stretch factor times Lewis number, KLe.

EXAMPLES OF ENGINE COMBUSTION MODEL USE

Four different examples of model use will now be given to illustrate both the potential of these various types of combustion models, and the engine combustion areas where they can provide valuable new insights. The topics chosen are: flame kernel development, the potential for flame quenching due to turbulent straining, causes of cycle-by-cycle combustion variability, and flow/flame interactions.

Flame Kernel Development

Herweg and Maly (11) have applied their combined flame structure (mean flame contour or front) and flame speed model (laminar, transition, and turbulent) to developing flame kernel data obtained from well-characterized experiments in a special transparent engine facility. Flame size was determined from schlieren photography. The flow field properties were determined by laser doppler velocimetry measurements and detailed three-dimensional modeling. Figure 13 shows predictions of flame radius as a function of time made with Eq. (27), compared with the measurements at three different relative air/fuel ratios (stoichiometric, λ = 1, and lean, λ = 1.3 and 1.5). Good agreement between predicted flame kernel growth and the measured growth is obtained.

A comparison of model predictions and measurements of the flame speed versus flame radius, over a range of engine speeds, provides insight into the processes which govern

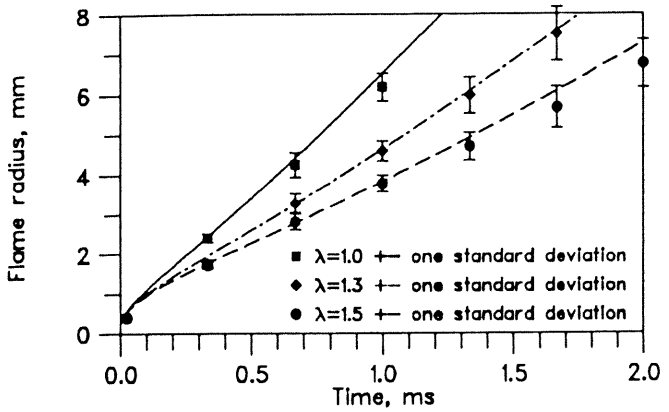

Fig 13: Comparison of predictions of flame radius versus time, made with the flame development model of Eq. (27), against experimental engine flame growth data (11). Engine speed 500 rev/min, part load, spark timing 10 deg. before top center, λ is the relative air/fuel ratio. Each data point represents average of 51 measured flame radii.

kernel growth. Results for central ignition are shown in Fig. 14, and again the agreement between model predictions and measurements is good (11). Initially, the flame expands rapidly, driven primarily by the high kernel temperatures generated by the energy in the electrical discharge, and also affected (negatively) by heat losses to the spark plug and flame-curvature produced strain. Then, the turbulence steadily speeds up the flame, this effect becoming greater, the higher the engine speed and the turbulence intensity. This study shows that these important physical processes can now be accurately described and modeled.

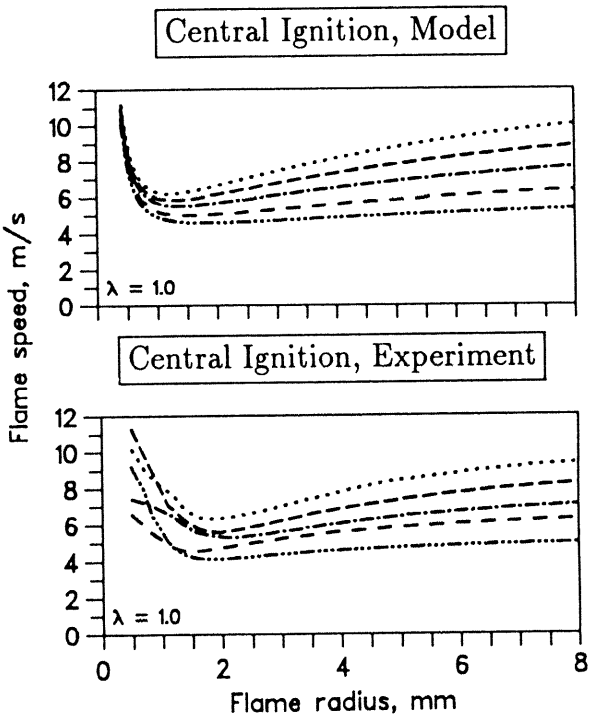

Fig. 14: Flame speed versus flame radius for the developing flame kernel, from model predictions and experiment, at different engine speeds, stoichiometric mixture, ignition in the center of the chamber, with a transistorized coil ignition system (11).

Turbulent Flame Straining

A recent application of the Leed's University flame speed model (20) (21), to the spark-ignition engine combustion process (17), provides useful insight into how the straining of the laminar flame due to wrinkling by the turbulence affects the flame propagation process. This study highlights where in the flame development and propagation process the flame is most susceptible to extinguishment by this straining. The engine combustion model used consisted of the entrainment and burn-up flame structure model (Eqs. (6) - (8)) combined with the flame speed model exemplified by Fig. 12.

Figure 15 shows, at the top, a comparison of the mass burned fraction versus crank angle profile predicted by the engine combustion model with the profile determined from the measured cylinder pressure data. Good agreement was obtained, as also was acceptable agreement between the mean flame radius and the detailed flame envelope shape and location data obtained by schlieren photography. The lower graph in Fig. 15 shows how the turbulent flame speed ratio, S_f / S_L, varies through the burning process, as a function of the effective turbulence intensity $u'k$, on a "Bradley diagram"

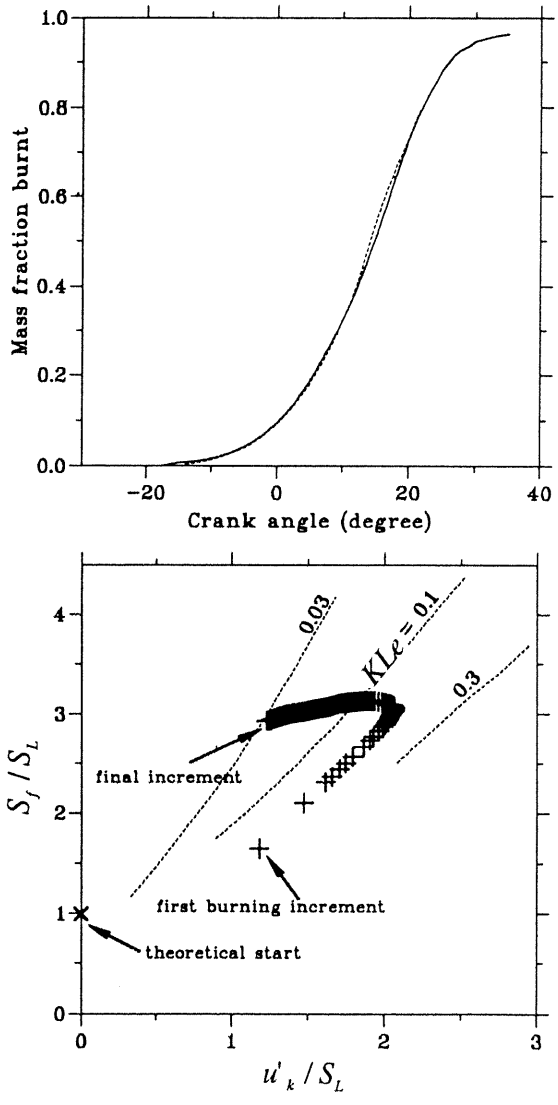

Fig. 15: Predictions of mass fraction burned versus crank angle (top graph), and of turbulent flame speed versus turbulence intensity (bottom graph) using the Leed's University flame speed model (17). Good agreement with burn rate data is obtained. Initially, the flame follows a path of constant *K*Le.

plot similar to Fig. 12. The flame grows, initially, along a line of essentially constant (KLe) as the flame experiences a wider range of the turbulence spectrum, which is what increasing u'_k corresponds to. Then, as the turbulence intensity levels off and decreases, and the laminar flame speed increases as the unburned mixture is compressed, the flame moves into regions of successively lower values of the Karlovitz stretch factor Lewis number product. Thus, the flame is most likely to quench in the early stages of its development when the value of (KLe) is high; this is in accord with experimental observations that flame kernel quenching occurs when the flame is a few mm in radius (25).

Cycle-By-Cycle Combustion Variations

A recent interesting application of a relatively complete entrainment and burn-up combustion model, within a quasi-dimensional engine cycle simulation, is explaining the causes of cycle-by-cycle combustion variations (34). Previous experimental research has identified several physical variables that affect the combustion process as being significant contributors to this variability. However, their relative significance is not known. By systematically introducing random variations into the combustion model inputs that control these parameters, the set of distributions of these parameters required to match the observed combustion statistics can be determined.

The experimental variations in critical combustion parameters 0 - 2 %, 0 - 10 %, 0 - 90 %, 10 - 90 % mass-fraction-burned angles, maximum cylinder pressure p_{max} and its crank angle of occurance θ_{pmax}, and imep, are shown in Fig. 16, at a light-load engine operating condition. At this load (imep = 1.7 bar), the combustion variability is substantial. The parameters varied in the combustion model were: (a) The distance the flame kernel center moves from the spark plug while it is small enough to be convected by the flow; this affects the magnitude of the flame envelope area as the flame grows and interacts with the combustion chamber walls. (b) The relative magnitude of the turbulence intensity, through variations in the coefficient C in Eq. (26); this affects the turbulent flame speed. (c) The size of the eddy within which the spark-generated flame kernel is embedded, accomplished by varying r_C in Eq. (26); this affects the timescale of the transition from the initial laminar to the eventual turbulent flame.

Figure 17 shows that a good match to the measured distributions in all these parameters can be obtained by variations in these three parameters of the appropriate amplitude. The phenomena these three parameters represent are all important contributors to cycle-by-cycle variations. Note that these three model variables are variables affected by different aspects of the in-cylinder flow field: flow velocity and turbulence scale in the vicinity of the spark plug, and the mean turbulence intensity in the cylinder.

Flow Flame Interactions

Understanding the interaction between the in-cylinder flowfield and the engine combustion process is especially important to developing an optimum combustion system. To date, most of this system development is done empirically because the appropriate modeling tools are not yet available. The following results from a multi-dimensional analysis of the spark-ignition engine combustion process illustrate how flame sheet models can be used to explore this flow/flame interaction

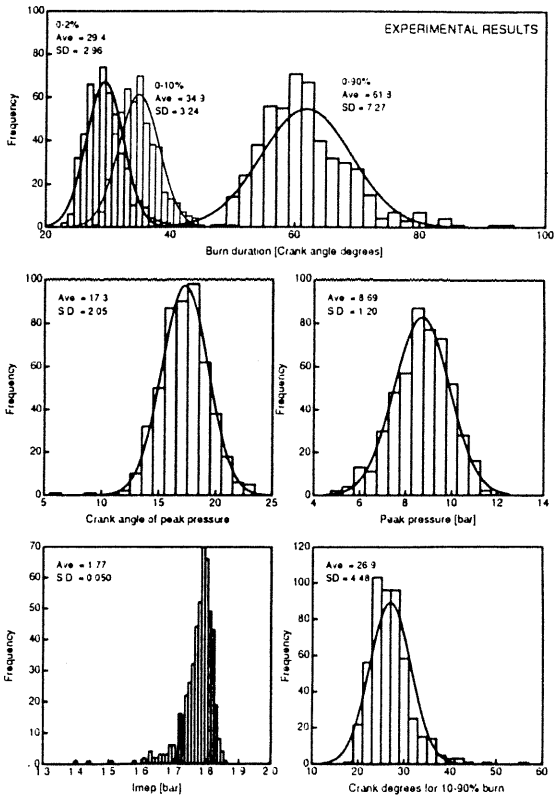

Fig. 16: Experimentally determined distributions of individual cycle values of 0 - 2 %, 0 -10 %, 0 - 90 %, 10 - 90 % mass burned angles, $\theta_{p\,max}$, p_{max}, and imep, at 750 rev/min and 1.77 bar imep for 500 cycles in a single cylinder Hydra engine (34).

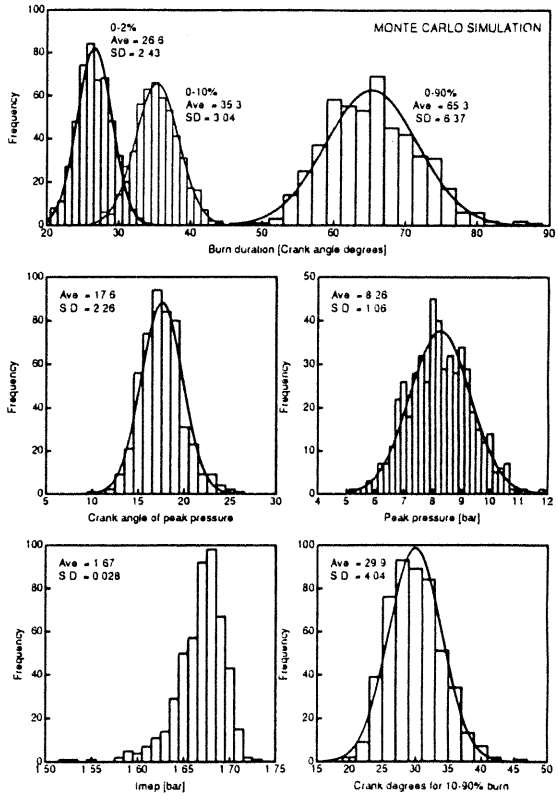

Fig. 17: Predicted distributions of the parameters shown in Fig. 16, made with an entrainment and burn up flame structure model in a quasi-dimensional engine simulation, with the parameters flame kernel center offset, turbulence intensity, and eddy size in which the spark discharge is embedded, randomly perturbed with a normal distribution and the appropriate standard deviation, to match the data in Fig. 16 (34). Good agreement is obtained.

(39). The flame structure model used is the coherent flame sheet model where the evolution of the flame sheet area per unit volume is described by Eqs. (18) and (19); the laminar flame speed model which that approach requires was that of Keck et al, Eqs. (20) and (21).

The geometry of the engine analyzed--a bowl-in-piston combustion chamber, and the success of the combustion rate prediction of the model, are shown in Fig. 18. The development of the measured cylinder pressure, and the mass fraction burned profile determined from it, are well matched by the predictions. Figure 19 shows details of the flame geomtry, early in its development, 17 crank angle degrees before TC. The top two figures show the product mass fraction contours, with essentially fully burned gas at the center of the flame, and a flame "brush" where the product mass fraction steadily decreases to zero. The bottom figure shows the flame sheet density contours. These are low on either side of the flame brush, with maximum values in the middle of the brush. Note that with this bowl-in-piston chamber geometry and an off-axis spark plug location, the complicated gas motion past the spark plug into the piston bowl, as the piston moves towards top center, significantly distorts the flame shape.

Other recent multi-dimensional model engine combustion calculations can be found in refs. (48)-(52). Only computational fluid dynamic models of the in-cylinder flow, coupled with an appropriate combustion model, can describe flow, flame, combustion chamber geometry interactions of this complexity.

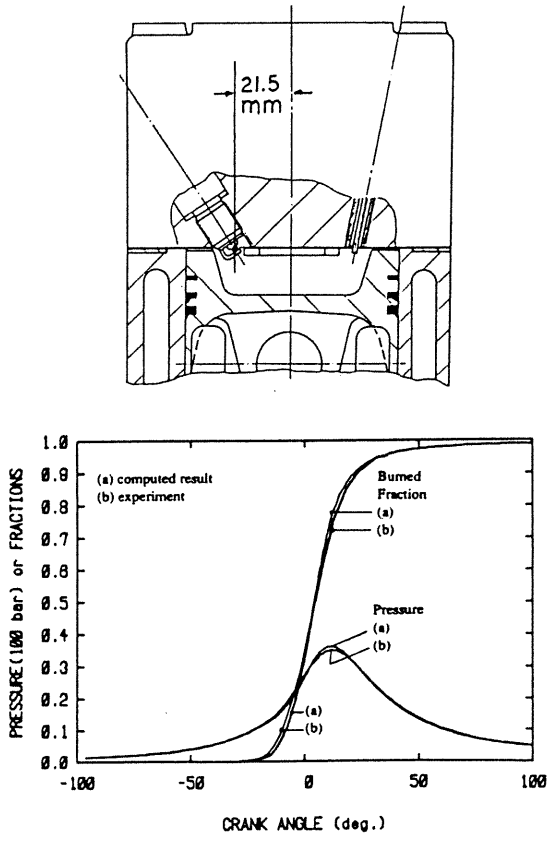

Fig. 18: Top geometry of spark-ignition engine combustion chamber studied (39). Bottom: comparison between predicted cylinder pressure and mass fraction burned versus crank angle profiles, and measurements. Good agreement was obtained.

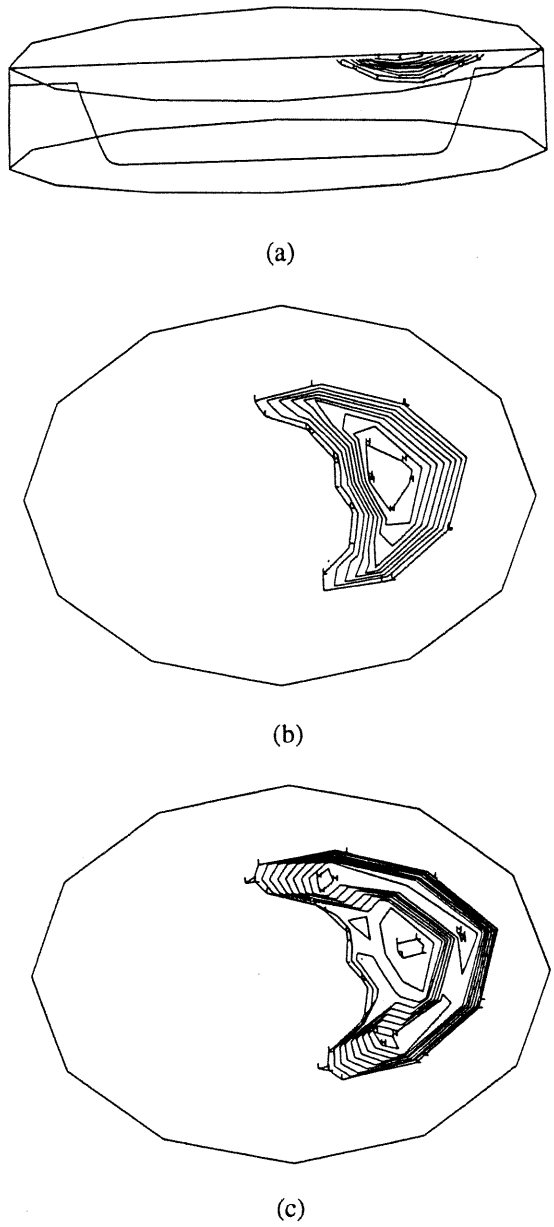

Fig. 19: Top and center: computed product mass fraction contours at 17 deg. BTC. The contour labels are H = 0.85, L = 0.094, and lines are plotted at intervals of 0.094: (a) azimuthal plane through the spark plug; (b) axial plane next to the head; (c) corresponding flame density contours in the axial plane next to the head; contour labels (in cm^{-1}) are H = 15.6, L = 1.74, and lines are plotted at intervals of 1.74 (39).

CONCLUDING COMMENTS

1. The past ten and more years of spark-ignition engine combustion research have been remarkably successful. Our understanding of the underlying physics has developed substantially, and the models developed which embody that physics now accurately predict many critical features of the engine combustion process.

2. The results of all this research have had a major impact on engine development and design. Modern "fast burn" combustion systems are as robust and effective as they now are due in large part to the knowledge base which combustion research has generated, and the computer simulations of engine operation which capture this knowledge in their combustion models.

3. There have been notable advances in our ability to quantify spark ignition, flame kernel growth and motion, the transition to a turbulent flame, the effects of strain, flame propagation speeds. These advances have been largely fluid dynamic based. Detailed modeling of the chemical processes occurring in the engine flame has, to date, had little direct impact on spark-ignition engine combustion modeling. Chemistry's role in engine flame propagation is still described via the laminar flame speed.

4. There remain several important engine combustion problems that we do not yet adequately understand. One is the spark discharge to flame kernel transition. A second is the flow, flame, combustion chamber geometry interaction, and especially the role of swirling and tumbling in-cylinder flows on the flame development and propagation processes. The third is the problem of cycle-by-cycle combustion variability and its role in defining engine operating limits. One important contributing factor to these unresolved problems is the fuel-air mixture preparation process. There is much research yet to be done.

REFERENCES

1. Heywood, J.B., "Internal Combustion Engine Fundamentals," Ch. 9, McGraw-Hill, New York, 1988.

2. Bracco, F.V., "Modeling and Diagnostics of Combustion in Spark-Ignition Engines," Proceedings of International Symposium on Diagnostics and Modeling of Combustion in Reciprocating Engines, COMODIA 85, Tokyo, Japan, pp. 1-13, September 4-6, 1985.

3. Pinchon, P., "Modeling of Fluid Dynamics and Combustion in Piston Engines," Proceedings of the International Symposium on Diagnostics and Modeling of Combustion in Internal Combustion Engines, COMODIA 90, Kyoto, Japan, pp. 31-47, September 3-5, 1990.

4. Maly, R., "Spark Ignition: Its Physics and Effect on the Internal Combustion Process," in J.C. Hilliard and G.S. Springer (eds.), Fuel Economy in Roads Vehicles Powered by Spark Ignition Engines, Chap. 3, Plenum Press, New York, 1984.

5. Pischinger, S. and Heywood, J.B., "A Study of Flame Development and Engine Performance with Breakdown Ignition Systems in a Visualization Engine, SAE paper 880518, SAE Trans., Vol. 97, 1988.

6. Ko, Y. and Anderson, R.W., "Electrode Heat Transfer During Spark Ignition," SAE paper 892083, SAE Trans., Vol. 98, 1989.

7. Pischinger, S. and Heywood, J.B., "How Heat Losses to the Spark Plug Electrodes Affect Flame Kernel Development in an SI-Engine," SAE paper 900021, SAE Trans., Vol. 99, pp. 53-73, 1990.

8. Boulouchos, K., Steiner, T, and Dimopoulos, P., "Investigation of Flame Speed Models for the Flame Growth Period During Premixed Engine Combustion," SAE paper 940476, 1994.

9. Beretta, G.P., Rashidi, M., and Keck, J.C., "Turbulent Flame Propagation and Combustion in Spark Ignition Engines," Combustion & Flame, Vol. 52, pp. 217-245, 1983.

10. Spicher, U. and Bäcker, H., "Correlation of Flame Propagation and In-Cylinder Pressure in a Spark Ignited Engine," SAE paper 902126, 1990.

11. Herweg, R. and Maly, R.R., "A Fundamental Model for Flame Kernel Formation in S.I. Engines," SAE paper 922243, SAE Trans., Vol. 101, 1992.

12. Winklhofer, E., Philipp, H., Fraidl, G., and Fuchs, H., "Fuel and Flame Imaging in SI Engines," SAE paper 930871, 1993.

13. Mantzaras, J, Felton, P.G., and Bracco, F.V., "Three-Dimensional Visualization of Premixed-Charge Engine Flames: Islands of Reactants and Products; Fractal Dimensions; and Homogeneity," SAE paper 881635, in SP-759, 1988.

14. Abraham, J., Williams, F.A., and Bracco, F.V., "Discussion of Turbulent Flame Structure in Premixed Charges," SAE paper 850345, 1985. Also in SAE P-156, 1985,

15. Liou, T.-M., Hall, M., Santavicca, D.A., and Bracco, F.V., "Laser Dopper Velocimetry Measurements in Valved and Ported Engines," SAE paper 840375, SAE Trans., Vol. 93, 1984.

16. Wirth, M., Keller, P., and Peters, N., "A Flamelet Model for Premixed Turbulent Combustion in SI-Engines," SAE paper 932646, 1993.

17. Merdjani, S. and Sheppard, C.G.W., "Gasoline Engine Cycle Simulation Using the Leeds Turbulent Burning Velocity Correlations," SAE paper 932640, 1993.

18. Heywood, J.B., "Combustion Chamber Design for Optimum Spark-Ignition Engine Performance," Int. J. of Vehicle Design, Vol. 5, No. 3, pp. 336-357, 1984.

19. Keck, J.C., Heywood, J.B., and Noske, G., "Early Flame Development and Burning Rates in Spark Ignition Engines," SAE paper 870164, SAE Trans., Vol. 96, 1987.

20. Abdel-Gayed, R.G., Bradley, D., and Lawes, M., "Turbulent Burning Velocities: A General Correlation in Terms of Straining Rates," Proc. R. Soc, London, A414, pp. 389-413, 1987.

21. Bradley, D., Lau, A.K., and Lawes, M., "Flame Stretch Rate as a Determinant of Turbulent Burning Velocity," Phil. Trans. R. Soc., London, A338, pp. 359-387, 1992.

22. Ziegler, G.F.W, Zettlitz, A., Meinhardt, P., Herweg, R., Maly, R., and Pfister, W., "Cycle-Resolved Two-Dimensional Flame Visualization in a Spark-Ignition Engine," SAE paper 881634, SAE Trans., Vol. 97, 1988.

23. Heywood, J.B., "Engine Combustion Modeling--An Overview," in Combustion Modeling in Reciprocating Engines, Editors: J.N. Mattavi & C.A. Amann, pp. 1-35, Plenum Press, 1980.

24. Bracco, F.V., "Introducing a New Generation of More Detailed and Informative Combustion Models, SAE paper 741174, 1974.

25. Pischinger, S. and Heywood, J.B., "A Model for Flame Kernel Development in a Spark-Ignition Engine," Proceedings of 23rd Symposium (Int'l) on Combustion,

Orleans, France, pp. 1033-1040, The Combustion Institute, 1990.

26. Refael, S. and Sher, E., "A Theoretical Study of Ignition of a Reactive Medium by Means of an Electrical Discharge," Combust. & Flame, Vol. 59, pp. 17-30, 1985.

27. Sher, E., Ben-Ya'ish, J., and Kravchik, T., "On the Birth of a Spark Channel," Comb. & Flame, Vol. 89, pp. 186-194, 1992.

28. Blizard, N.C. and Keck, J.C., "Experimental and Theoretical Investigation of Turbulent Burning Model for Internal Combustion Engines," SAE paper 740191, SAE Trans., Vol. 83, 1974.

29. Tabaczynski, R.J., Ferguson, C.R., and Radhakrishnan, K., "A Turbulent Entrainment Model for Spark-Ignition Engine Combustion," SAE paper 770647, SAE Trans., Vol. 86, 1977.

30. Tabaczynski, R.J., Trinker, F.H., and Shannon, B.A.S., "Further Refinement and Validation of a Turbulent Flame Propagation Model for Spark-Ignition Engines," Comb. & Flame, Vol. 39, pp. 111-121, 1980.

31. Keck, J.C., "Turbulent Flame Structure and Speed in Spark-Ignition Engines," Proceedings of Nineteenth Symposium (Int'l) on Combustion, pp. 1451-1466, The Combustion Institute, 1982.

32. Davis, G.C., Tabaczynski, R.J., and Belaire, R.C., "The Effect of Intake Valve Lift on Turbulence Intensity and Burnrate in S.I. Engines-Model Versus Experiment," SAE paper 840030, SAE Trans., Vol. 93, 1984.

33. Davis, G.C., Mikulec, A., Kent, J.C., and Tabaczynski, R.J., "Modeling the Effect of Swirl on Turbulence Intensity and Burn Rate in S.I. Engines and Comparison with Experiment," SAE paper 860325, SAE Trans., Vol. 95, 1986.

34. Brehod, D.D., and Newman, C.E., "Monte Carlo Simulation of Cycle by Cycle Variability," SAE paper 922165, 1992.

35. Gouldin, F.C., "An Application of Fractals to Modeling Premixed Turbulent Flames," Comb. & Flame, Vol. 68, pp. 249-266, 1987.

36. Santavicca, D.A., Liou, D., and North, G.L., "A Fractal Model of Turbulent Flame Kernel Growth," SAE paper 900024, SAE Trans., Vol. 99, 1990.

37. Matthews, R.D. and Chin, Y-W., "A Fractal-Based SI Engine Model: Comparisons of Predictions with Experimental Data," SAE paper 910079, SAE Trans., Vol. 100, 1991.

38. Wu, C-M., Roberts, C.E., Matthews, R.D., and Hall, M.J., "Effects of Engine Speed on Combustion in SI Engines: Comparisons of Predictions of a Fractal Burning Model with Experimental Data," SAE paper 932714, 1993.

39. Cheng, W.K. and Diringer, J.A., "Numerical Modeling of SI Engine Combustion with a Flame Sheet Model," SAE paper 910268, SAE Trans., Vol. 100, 1991.

40. Pope, S.B., "The Statistical Theory of Turbulent Flames," Phil. Trans. R. Soc. Lon. A291, 1979.

41. Bray, K.N.C. and Moss, J.B., "A Unified Statistical Model of Premixed Turbulent Flames," Acta Astronaut. 4, 1977.

42. Borghi, R., Arguerolles, B.S., and Souhaite, P., "Application of a Presumed pdf Model of Turbulent Combustion to Reciprocating Engines," Proceedings of 21st Symp. (Int'i) on Combust., The Combustion Institute, 1987.

43. Metghalchi, M. and Keck, J.C., "Laminar Burning Velocity of Propane-Air Mixtures at High Temperature and Pressure," Combust. Flame, Vol. 38, pp. 143-154, 1980.

44. Metghalchi, M. and Keck, J.C., "Burning Velocities of Mixtures of Air with Methanol, Iso-octane, and Indolene at High Pressure and Temperature," Comb. & Flame, Vol. 48, pp. 191-210, 1982.

45. Rhodes, D.B., and Keck, J.C., "Laminar Burning Speed Measurements of Indolene-Air-Diluent Mixtures at High Pressures and Temperature," SAE paper 850047, SAE Trans., Vol. 94, 1985.

46. Gülder, Ö.L., "Correlations of Laminar Combustion Data for Alternative S.I. Engine Fuels," SAE paper 841000, 1984.

47. Markstein, G.H., "Non-Steady Flame Propagation, Pergamon Press, New York, 1964.

48. Kuo, T-W., "Multidimensional Port-and-Cylinder Gas Flow, Fuel Spray, and Combustion Calculations for a Port-Fuel-Injection Engine," SAE paper 920515, SAE Trans., Vol. 101, 1992.

49. Mantel, T., "Three Dimensional Study of Flame Kernel Formation Around a Spark Plug," SAE paper 920587, SAE Trans., Vol. 101, 1992.

50. Naitoh, K., Itoh, T, Takagi, Y., and Kuwahara, K., "Large Eddy Simulation of Premixed-Flame in Engine Based on the Multi-Level Formulation and the Renormalization Group Theory," SAE paper 920590, SAE Trans., Vol. 101, 1992.

51. Boudier, P., Henriot, S., Poinsot, T., and Baritaud, T., "A Model for Turbulent Flame Ignition and Propagation in Spark Ignition Engines," Twenty-Fourth Symposium (Int'l) on Combution, The Combustion Institute, pp. 503-510, 1992.

52. Zhao, X., Matthews, R.D., and Ellzey, J.L., "Three-Dimensional Numerical Simulation of Flame Propagation in Spark Ignition Engines," SAE paper 932713, 1993.